
Article:
Goff, J.E., Boswell, L., Ura, D. et al. (2 more authors) (2018) Critical shoe contact area ratio for sliding on a tennis hard court. Proceedings of the Institution of Mechanical Engineers, Part P: Journal of Sports Engineering and Technology , 232 (2). pp. 112-121. ISSN 1754-3371

https://doi.org/10.1177/1754337117715341

Critical shoe contact area ratio for sliding on a tennis hard court

Journal of Sports Engineering and Technology
XX(X):1–11

DOI: 10.1177/ToBeAssigned
www.sagepub.com/
SAGE

John Eric Goff,[1] Luke Boswell,[2] Daniel Ura,[2] Mark Kozy,[1] and Matt J Carré[2]

Abstract

Dimples have been used in the design of some modern tennis shoe outsoles to enhance sliding ability on hard courts. Experiments were performed with bespoke rubber samples possessing various numbers of holes, which served to simulate dimples in tennis shoe treads, the aim being to assess the effect of contact area on sliding friction. It was found that as the ratio of holes to solid rubber increases, a critical ratio is reached whereby the static friction coefficient drops by more than 11% for tread-to-court pressures comparable to real tennis play. Though experiments reported here concern bespoke rubber samples, shoe manufacturers should be interested in the appearance of a critical dimple ratio that could aid them in the creation of tennis shoes suited for sliding on hard courts.

Keywords

friction, static friction, kinetic friction, shoe treads, mechanical test device

[1]Department of Physics, Lynchburg College Lynchburg, VA, 24501, USA
[2]Department of Mechanical Engineering, University of Sheffield, S1 3JD, UK

Corresponding author:
John Eric Goff, Department of Physics, Lynchburg College, 1501 Lakeside Drive, Lynchburg, VA, 24501, USA.
Email: goff@lynchburg.edu

Prepared using sagej.cls *[Version: 2015/06/09 v1.01]*

Nomenclature

a	Acceleration
F_{ram}	Pneumatic ram force (magnitude)
f_s	Static friction force (magnitude)
f_k	Kinetic friction force (magnitude)
F_N	Normal force (magnitude)
g	Acceleration due to gravity (magnitude)
LVDT	Linear Variable Displacement Transducer
PPR	Portable Prototype Rig
μ_s	Coefficient of static friction
μ_k	Coefficient of kinetic friction
y, z	Fitting parameters for μ_s
σ_y, σ_z	Standard errors for y, z

Introduction

The evolution of tennis shoes has been influenced by the court surface and the complexity of player movements. In the search to reduce injury risk and enhance player performance, shoe manufacturers have designed tennis shoes specific to each surface (grass, clay, and hard court). Previous work [1] has shown how tread geometry and orientation affect the size of the friction force in a typical shoe-surface interface.

Early tennis shoes were comprised of a flat, rubber sole, complemented with a canvas or leather upper section fastened with laces. One of the first specialized shoes used in tennis was the "plimsoll," in which rubber was attached to the upper part of the shoe. [2] These shoes became popular for grass tennis courts and sole patterns were added (and patented) to add grip and court adhesion. A second example of one of the most technologically advanced performance tennis shoes on the market was the Haillet shoe, introduced in 1969 to provide more grip on a tennis surface, thanks to its rubber cup sole with herringbone profile treads. [3]

Rather than focusing only on protection, today's tennis shoe designers make use of biomechanics, sophisticated materials, textiles, and sole designs to merge foot support and protection to enhance player performance. Shoes are further designed according to the mechanical properties of a given playing surface, from hard to resilient, with different amounts of friction that allow players to have grip, cushioning, and stability during complex dynamic movements on a tennis court.

Although there are specific shoes designed to play tennis on the three main surfaces, there are not many official regulations from the International Tennis Federation about the shoes used on each surface.

A general rule is that shoes shall not cause damage to the court other than what is expected during the normal course of a match or practice.[4]

The principal difference between shoes designed for each surface is the tread pattern that is used. From smooth soles for indoor carpets, to zig zag or herringbone patterns for clay or hard courts, to pimpled treads for grass courts, designs have specialized according to player-surface needs. In a tennis shoe survey[5] 1524 competitive tennis players from China, USA, and Germany provided their perspectives on tennis footwear by answering questionnaires. Regardless of country of origin and skill level, the most important shoe properties were fit, comfort, traction, injury protection, and outsole durability. These observations have provided evidence-based guidance for shoe manufacturers of tennis footwear design in terms of players' needs.

An example of revolutionary innovation is the circular design pattern incorporated into the tread to create pivot points where rotational friction is reduced with the goal of reducing injuries.[6] Some manufacturers have designed their outsoles with various geometries and tread orientations, such as a shoe created by inventors[7] for which the sole was designed with knowledge of the stresses exerted by top-level players, whose performances depend on the quality and variety of reactions with the playing surface. The sole's main section contains a sculpted pattern having recesses and solid areas. The shoe manufacturer claims,[7] "the recesses and solid areas are distributed to minimize pressures or stress differences throughout the ground engagement section concerned so as to provide better adherence and lower wear by abrasion in response to such mode of solicitations." These sole features help players make use of different parts of the shoe's outsole as needed, depending on the playing surface and movement. More grip while initiating running and sliding on clay to reach a ball faster are examples of typical movements performed by players on a tennis court.

Thanks to technological developments, tennis pace has increased.[8–10] Players have thus developed stronger and faster movements on court to react to an incoming ball, such as during a serve. Players must also reposition more quickly in preparation for return shots. Increased ball speed[9] may explain why some players have started sliding on hard courts,[11] meaning sliding is no longer the exclusive purview of clay-court play. An example of this technological improvement is the "Wilson Glide" shoe. It was developed on the concept of clay sliding, but its revolutionary design allows players to slide on hard courts.[12] The "Wilson Glide" contains a strategically-placed plastic plate slightly recessed into the outsole that allows players to slide more easily than with a traditional shoe. To use the shoe effectively a player must learn to use the glide plate to successfully execute a slide on a tennis hard court.

A possible disadvantage of the "Wilson glide" shoe is that players must become acclimated to the sliding technique required by the shoe. It was reported in a previous study[11] that the "Wilson glide" shoe could help reduce players' reposition time when sliding on hard courts compared to performing traditional adjustments. A total of 18 male tennis players of "good" ability were filmed playing a series

balls while wearing the new shoes and additional series of balls while wearing regular shoes. Results showed that the time for reposition was reduced by 42% when wearing the new shoes compared to regular shoes.

Shoes designed for sliding appear to make use of dimples (recessed areas) instead of a pimpled tread (with protruding areas). Figure 1 shows a photo of the outsole of such a design, the Babolat Men's Propulse 4 All Court Tennis Shoe that was used in this study for comparison. The work described in this paper focuses on dimple patterns, the aim being to investigate how the ratio of dimples to rubber influences the frictional interaction between shoe and court surface. We hypothesized that the higher the ratio of dimples to rubber, the lower the coefficient of friction. Comparisons with results from treads manufactured in house will be made in the **Results and Discussions** section.

Figure 1. Photograph of the outsole of a popular Babolat shoe. Region 1 contains pimples; Region 2 contains dimples. Region 2 is the area of interest in this work. The oval-shaped dimples measure $6.3\,\text{mm} \times 12.1\,\text{mm}$. Both regions contain portions of a white rubber S pattern.

Experimental Techniques

Testing took place using the bespoke portable prototype rig (PPR), developed and fully described elsewhere.[13] The PPR is a smaller and more portable version of an earlier rig.[14] Annotated photographs of the experimental setup are shown in Figure 2. The PPR consists of five main sections: (1) the pneumatic ram and its connections, (2) the load cell, (3) the slider, (4) four 10-kg masses, and (5) the linear variable displacement transducer (LVDT). The tread sample to be tested was fixed onto the bottom of the slider using adhesive tape and screws as shown in the bottom right of Figure 2. The slider was then fixed onto the connections, directly underneath the normal force loading area. The system was loaded with the appropriate number of 10-kg masses to achieve the desired normal force. One, two, three, and four 10-kg masses were used to achieve normal forces of 104.5 N, 202.6 N, 300.7 N, and 398.8 N, respectively. These normal forces take into account the mass of the connections (0.652 kg), which was determined using an Ohaus Scout 2 Digital Lab Balance. The pneumatic ram's maximum driving pressure was set at 2 bar.

The pneumatic ram provided the horizontal force and caused the slider and tread sample to slide across the surface with a displacement of 10 cm. This method contrasts that of other work [15;16] where the tread is held stationary and the surface is moved. The load cell and LVDT provided data necessary to analyze the slide. The load cell measured the ram force and the LVDT measured displacement, each sampled at a frequency of 1666.67 Hz, meaning data were collected in 0.0006-s intervals. Tests were randomized by using different parts of the court surface for each trial. The surface was cleaned before each trial to remove rubber buildup.

Because sliding necessarily requires that friction passes from the static regime to the kinetic regime, the initial action of the ram led to a forward pitching moment on the slider. That meant that the rubber samples did not have the uniform contact with the tennis surface while sliding that they possessed before the ram was engaged. The leading edge of the sample thus showed more wear over time compared to the back edge. No method has yet been discovered that allows for even wear across the patch of area that is initially in contact with the tennis surface. Nonuniform wear meant that special care had to be taken to determine the contact area between sample and tennis court surface. The method used to find the contact area will be described shortly.

As other investigations [1;17] have used, shoe treads were simulated with commercially-available rubber. Seven bespoke samples were produced from N70 Nitrile Butadiene Rubber, each with a different area ratio; they are shown in Figure 3. The manufacturer's specified values for the rubber's shore hardness (71, Shore A), tensile strength (14 MPa), and elongation at break (385%) are all consistent with the rubber found on a typical tennis shoe. [13]

The area ratio is defined as the hole area within the contact area divided by the contact area plus hole area. Figure 4 shows a typical patch of contact area and offers a visualization of how the area ratio is defined. The smooth sample obviously has zero area ratio because the sample has no holes. A nonphysical sample completely covered with holes and having no rubber, i.e. nothing, would have unit area ratio. We use this convention because we are referring to hole area instead of contact area and how the number of dimples (holes) effect sliding on hard courts.

Instead of using a static ink blot to determine contact area, [18] a new method is introduced here. To calculate the area ratio, a boundary of known dimensions was set around the wear regions of each sample after testing and photographs were taken under appropriate lighting conditions to show contrast between the regions of wear and regions showing no wear. Figure 5 shows five of the seven samples tested. Images were then processed via thresholding. Black pixels represented the wear region and that region's area was found by calculating the percentage of black pixels in the overall image. The wear region is the maximum possible contact area that could occur during testing because no one test is likely to wear the sample in the same way as another test. It is the accumulation of all tests that leads to the final wear pattern. To find the area ratio, the number of holes within each wear region was counted. Tread samples 1

and 6, regrettably, could not be assessed using this method because extra testing took place on those two samples before photographs could be taken. The wear area of sample 1 was assumed to be the same as sample 2, excluding the holed area. The wear area and area ratio of sample 6 were found by interpolating the data across all area ratios. Videos taken during a few trials indicated that any tipping due to a forward moment on the slider took place at the start of movement and not during movement.

Each sample was tested at the aforementioned normal loads of 104.5 N, 202.6 N, 300.7 N and 398.8 N, at an angle with the horizontal of 0° with five tests for each condition, leading to a total of 20 tests for each sample. Samples slid on an acrylic hard-court tennis surface supplied by the International Tennis Federation. The roughness of the surface ($\mathrm{Ra} = 10.73\,\mu\mathrm{m} \pm 1.44\,\mu\mathrm{m}$) was measured with a Mitutoyo Surftest SJ-400 Profilometer.

The coefficient of static friction, μ_s, was found just prior to the test sample moving. The pneumatic ram's applied force, F_{ram}, matches the static friction force's magnitude, f_s, prior to the sample's movement. Given knowledge of the normal force, F_N, and the measured values of the ram's force, the coefficient of static friction was found from

$$\mu_s = f_s / F_N \,. \tag{1}$$

Newton's second law equation must be employed to determine the coefficient of kinetic friction, μ_k. The sample moved over a distance of 10 cm before the ram was fully extended. Because the sample began at rest and came to rest after 10 cm of movement, the sample must have accelerated. That means that the magnitude of the ram's force did not equal the magnitude of the kinetic friction force, defined as

$$f_k = \mu_k \, F_N \,. \tag{2}$$

Newton's second law equation gives

$$\mu_k = F_{ram} / F_N - a/g \,, \tag{3}$$

where the magnitude of the gravitational acceleration is $g = 9.81\,\mathrm{m/s^2}$. After getting position data from the LVDT, the sample's acceleration, a, was found by first smoothing the position data and then evaluating two numerical time derivatives. The sample's speed, v, was obtained from one numerical time derivative of the smoothed position data, meaning the coefficient of kinetic friction as a function of speed was found. Preventing unwanted movement in the PPR at the beginning and end of the sample's motion from adversely influencing kinetic friction calculations was achieved by considering only position data between 2 cm and 8 cm for the ram's extension. To keep upcoming plots of μ_k versus v from being too

cluttered, μ_k values from each of the five tests at a given normal force and at a given speed were averaged, leading to a single plot of μ_k versus v for a given normal force.

Results and Discussion

Figures 6–12 show coefficient of static friction versus normal force and coefficient of kinetic friction as a function of speed for the seven samples under investigation. Raw data are shown on the static friction plots, as well as curves best fit to the data. Static friction data are fitted to the following function, similar to what has been used before [19;20] for coefficients of kinetic friction,

$$\mu_s = y/\tilde{F}_N^z \,, \tag{4}$$

where $\tilde{F}_N = F_N/(1\,\mathrm{N})$ is dimensionless and ensures that besides the exponent z, the factor y is dimensionless. Examination of the data in Figures 6–12 led to the choice of the power-law fit given in equation (4).

Table 1 contains the static friction fitting parameters, y and z, and their associated standard errors, δy and δz, respectively, for the seven samples. Figure 13 shows the fitting functions given by equation (4)

Table 1. Static friction fitting parameters.

Sample	$y \pm \delta y$	$z \pm \delta z$
1	7.748 ± 0.554	0.323 ± 0.014
2	9.827 ± 1.132	0.363 ± 0.022
3	8.441 ± 1.056	0.336 ± 0.024
4	10.211 ± 1.659	0.366 ± 0.031
5	10.526 ± 1.122	0.394 ± 0.020
6	12.677 ± 1.497	0.425 ± 0.023
7	9.304 ± 1.261	0.377 ± 0.026

and Table 1. Below about $F_N = 200\,\mathrm{N}$, the fitting functions are not separated from each other in any distinguishable way. The spread in data for small normal forces as seen in Figures 6–12 is responsible for the lack of distinguishability and is indirectly due to stick-slip phenomena. Stick-slip phenomena are easily seen in high-speed video while the samples are in motion. Even though static friction coefficients are determined just prior to the samples moving, each experimental test cannot be performed by starting the sample in exactly the same place. Microscopic chemical bonds giving rise to macroscopic static friction are not easily repeated with small normal forces and differing starting positions. By covering different numbers of surface asperities in different ways, static friction is inevitably altered from one trial

to the next. As the normal force increases, however, contact between sample surfaces and the hard court surface is more consistent between trials.

The normal force was chosen as an independent variable instead of the pressure because what is imagined is a tennis player of a given weight choosing one shoe over another. In other words, for a given normal force, how does friction change as the area ratio changes? What has been discovered in the plots of μ_s versus F_N is that for large values of F_N there is a drop in μ_s as the area ratio passes some critical value. Samples 1–4 (area ratios, 0.000 to 0.227; see Figure 3) give comparable static friction coefficients for normal forces greater than about 300 N. The same may be claimed for samples 5–7 (area ratios, 0.288 to 0.373; see Figure 3).

To further illustrate the appearance of a critical area ratio, consider Figures 14–15. The standard error bars in Figure 14 are such that average values of μ_s are not statistically different, though the onset of a separation effect is seen in the plot with the 20-kg mass attached. Figure 15 shows that the μ_s values for samples 1–4 are clearly different from the μ_s values for samples 5–7. The standard error bars for samples 1–4 do not overlap those of samples 5–7. When the 30-kg mass was attached, the average value of μ_s for samples 5–7 drops by 11% from the average value of μ_s for samples 1–4; the drop in average μ_s was 13% when the 40-kg mass was used. There is thus a critical area ratio between 0.227 and 0.288 where the coefficient of static friction drops for normal forces approaching that seen by a tennis player sliding on a hard court.

The critical area ratio's appearance is made even more definitive with an in-depth Analysis of Variance[21] (ANOVA) study. All ANOVA calculations were performed using the software *Mathematica*.[22] The Tukey post-hoc test was performed at the 5% confidence level for each normal force. Only for the application of the 30-kg and 40-kg masses were μ_s values for samples 1–4 significantly different from samples 5–7. For both tests, $p < 10^{-6}$. The visual suggestion in Figure 15 is thus confirmed via ANOVA. At the top two normal forces used in this study, μ_s values associated with the area ratios for samples 1–4 are significantly different from μ_s values associated with the area ratios for samples 5–7. There is thus a statistically significant change in μ_s for large normal force as the area ratio moves from that of sample 4, namely 0.227, to the area ratio for that of sample 5, namely 0.288, which suggests the presence of a critical area ratio between 0.227 and 0.288.

Babolat manufactures a commercially-available all-court tennis shoe called "Babolat Men's Propulse 4 All Court Tennis Shoe (Orange)" with pimples over most of its bottom surface, but dimples located on the outer part of its bottom surface. Recall Figure 1. The area ratio for the dimpled portion is about 0.35, putting it close to sample 6 that was studied here. Figure 13 shows the best-fit curve for the Babolat sample tested in a previous study.[1] For the Babolat's area ratio, the coefficient of static friction curve is with samples 5–7 for large normal forces. The dimpled pattern on the outer part of the bottom surface

of the Babolat shoe thus suggests the possibility of sliding on hard court over a dimpled pattern with a smaller area ratio.

Though normal force was emphasized over pressure in this work, pressures were easily determined once contact areas were found. Focusing only on the transition region, with 30-kg masses attached, pressures on Samples 4 and 5 were about 744 kPa and 763 kPa, respectively. With 40 kg attached, those pressures rose to 987 kPa and 1012 kPa. The aforementioned pressures exceed the nearly 600 kPa other research[23] found to be typical peak pressures during normal tennis play. Sliding on a clay court has been measured[24] to be approximately 200 kPa. But sliding on clay is much easier than sliding on a hard court. It is not surprising that sliding on a hard tennis court with only the outside portion of a player's outsole in contact with the court could lead to peak pressures in excess of 600 kPa.

Other more general comments may be made by observing Figures 6–12. The coefficient of static friction clearly decreases with normal force. And for a given normal force, $\mu_s > \mu_k$, as expected. From the plots of μ_k versus F_N, it is clear that as normal force increases, speed goes down because of the increased difficulty in moving the slider for a fixed pneumatic ram pressure. For both μ_s and μ_k, data are more compact as F_N increases. Though the averaged coefficient of kinetic friction curves are rather erratic in places, it is easy to obtain an estimate of the approximate value of μ_k for a sample and normal force. Note, too, that coefficients of kinetic friction are roughly the same for all samples tested. Because tested speeds were small (< 0.4 m/s), results here refer to an actual tennis shoe near the end of its slide. No matter the area ratio, it appears that holed treads will behave in approximately the same way as the athlete's slide brings him or her to rest.

Conclusions and Future Work

Having a critical area ratio between 0.227 and 0.288 should be of great interest to tennis shoe manufacturers. Sliding is no longer restricted to clay-court play. Elite players we have watched, like Novak Djokovic, have already shown they can effectively slide on hard courts. The portion of the Babolat shoe mentioned in the previous section has an area ratio above the critical value, suggesting the possibility that the shoe is effective at allowing for hard-court sliding on the outer portion of the bottom of the shoe. Future work could extend this by incorporating human biomechanical testing of different outsole designs.

Understanding on a more fundamental level what is happening as the area ratio passes its critical value will occupy part of future work. It will also be interesting to break the hole symmetry and use different dimple shapes, much like the ovals on the Babolat shoe. Breaking symmetry and moving the tread in different directions leads to different static friction coefficients.[1] It will have to be determined if the different oval orientations are responsible, if the white rubber (see Figure 1) is responsible, or if a combination of the two is responsible. There may also be a systematic difference in the way

measurements were made[1] at different orientation angles, and such a difference will have to be fleshed out in future work.

Future work will also investigate ways of studying the sliding samples at larger speeds to better understand the coefficient of kinetic friction at speeds comparable to those encountered by tennis players at the beginning of their slides. Work presented here could only get sliding speeds within an order of magnitude of the roughly 4 m/s experienced by a tennis player's shoe during its initial slide.[25] Coefficients of kinetic friction are roughly the same for all samples tested but the tested speeds were small (< 0.4 m/s) - similar to what an actual tennis shoe experiences near the end of its slide. Therefore, no matter the area ratio, it appears that the holed treads as tested in this study would behave in approximately the same way as the athlete's slide brings him or her to rest.

We also hope to incorporate player perceptions into our future research. Building on past similar work,[26] we wish to determine if professional tennis players notice a difference in a shoe's sliding ability as the critical area ratio changes through the critical zone uncovered in this work. As players use shoes of various area ratios, we will also check to see if area ratio affects a shoe's durability. As holes get larger, smaller protrusions may be easier to break off during movement.

Acknowledgements

The authors extend a special thank you to Jamie Booth for assisting in the creation of the PPR and the samples used in this study. The International Tennis Federation is also thanked for generous financial support. The authors finally thank this paper's three referees, who each provided incredibly valuable feedback that greatly enhanced the quality of this paper.

References

1. Goff JE, Ura D, Boswell L, and Carré MJ. Parametric study of simulated tennis shoe treads. *Proc Eng* 2016; 147:443-448.
2. Keyser A. *Sneaker Century: A History of Athletic Shoes*. Minneapolis, MN: Learner Publishing Group, 2015.
3. Haillet Shoe (homepage on the Internet), https://www.adidas-archive.org/ourheroes /smith (2016, accessed 13 June 2016).
4. Rules of Tennis (homepage on the Internet), http://www.itftennis.com/media/221030 /221030.pdf (2016, accessed 24 Feb 2016).
5. Sterzing T, Barnes S, Althoff K, Determan L, Liu H, and Cheung JTM. Tennis shoe requirements in China, USA, and Germany. *Footwear Science* 2014; 6: 165-176.
6. Anderie W. Sports shoes, France. US patent 4,281,467 (4 August 1981).
7. Jara A, Larregain A, and Perrin F. High-performance sports shoe. US patent US2010/0170114A1 (8 July 2010).

8. Haake SJ, Chadwick SG, Dingnall RJ, Goodwill S, and Rose P. Engineering tennis – slowing the game down. *Sports Engineering* 2000; 3: 131-143.
9. Miller S. Modern tennis rackets, balls, and surfaces. *British Journal of Sports Medicine* 2006; 40: 401-405.
10. Haake S, Allen T. Choppin S, and Goodwill S. The evolution of the tennis racket and its effect on serve speed. *Tennis Science and Technology 3*. London: International Tennis Federation, 257-271, 2007.
11. Pavailler S and Horvais N. Sliding allows faster repositioning during tennis specific movements on hard court. *Engineering of Sport 10* 2014; 72: 859-864.
12. Glide Shoe (homepage on the Internet), http://www.wilson.com/dyn/racquet/glide (2016, accessed 17 April 2016).
13. Ura D and Carré MJ. Development of a novel portable test device to measure the tribological behaviour of shoe-court interactions in tennis. *Proc Eng* 2016; 147:550-555.
14. Clarke J, Carré MJ, Damm L, and Dixon S. The development of an apparatus to understand the traction developed at the shoe-surface interface in tennis. *J Sports Eng and Tech* 2012; 227: 149-160.
15. Adam CS and Piotrowski M. Use of the unified theory of rubber friction for slip-resistance analysis in the testing of footwear outsoles and outsole compounds. *Footwear Science* 2014; 4: 23-35.
16. Blanchette MG and Power CM. The influence of footwear tread groove parameters on available friction. *Applied Ergonomics* 2015; 50: 237-241.
17. Li KW, Wu HH, and Lin YC. The effect of shoe sole tread groove depth on the friction coefficient with different tread groove widths, floors and contaminants. *Applied Ergonomics* 2006; 37: 743-748.
18. Ura D, Caballero J, and Carré M. Tennis shoe-court interactions: examining relationships between contact area, pressure, and available friction. *Footwear Science* 2015; 7: S87-S89.
19. Clarke J, Carré MJ, Richardson A, Yang Zhijun, Damm L, and Dixon S. Understanding the traction of tennis shoes. *Proc Eng* 2011; 13: 402-408.
20. Clarke J, Carré MJ, Damm L, and Dixon S. Understanding the influence of surface roughness on the tribological interactions at the shoesurface interface in tennis. *Proc Inst of Mech Eng, Part J: J of Eng Trib* 2012; 226: 636-647.
21. Bird K. *Analysis of Variance Via Confidence Intervals*. London, UK: SAGE Publications Ltd, 2004.
22. Mathematica (homepage on the Internet), http://www.wolfram.com/mathematica/ (2016, accessed 26 September 2016).
23. Damm L, Starbuck C, Stocker N, Clarke J, Carré M, and Dixon S. Shoe-surface friction in tennis: influence of plantar pressure and implications for injury. *Footwear Science* 2014; 6: 155-164.
24. Bloch O, Potthast W, and Brüggemann GP. Pressure Distribution During Sliding on Tennis Clay Court. *Proc Fourth Symposium on Footwear Biomechanics* 1999; 4: 26-27.
25. Ura D, Carré MJ, Charlton H, Capel-Davies J, Miller S, Sanchis Almenara M, Astiz J, and de Alfonso Mustienes A. Influence of clay properties on shoe-kinematics and friction during tennis movements. *Proc Eng* 2014; 72:

889-894.

26. Starbuck C, Damm L, Clarke J, Carré M, Capel-Davis J, Miller S, Stiles V, and Dixon S. The influence of tennis court surfaces on player perceptions and biomechanical response. *J of Sports Sci* 2016: 34; 1627-1636.

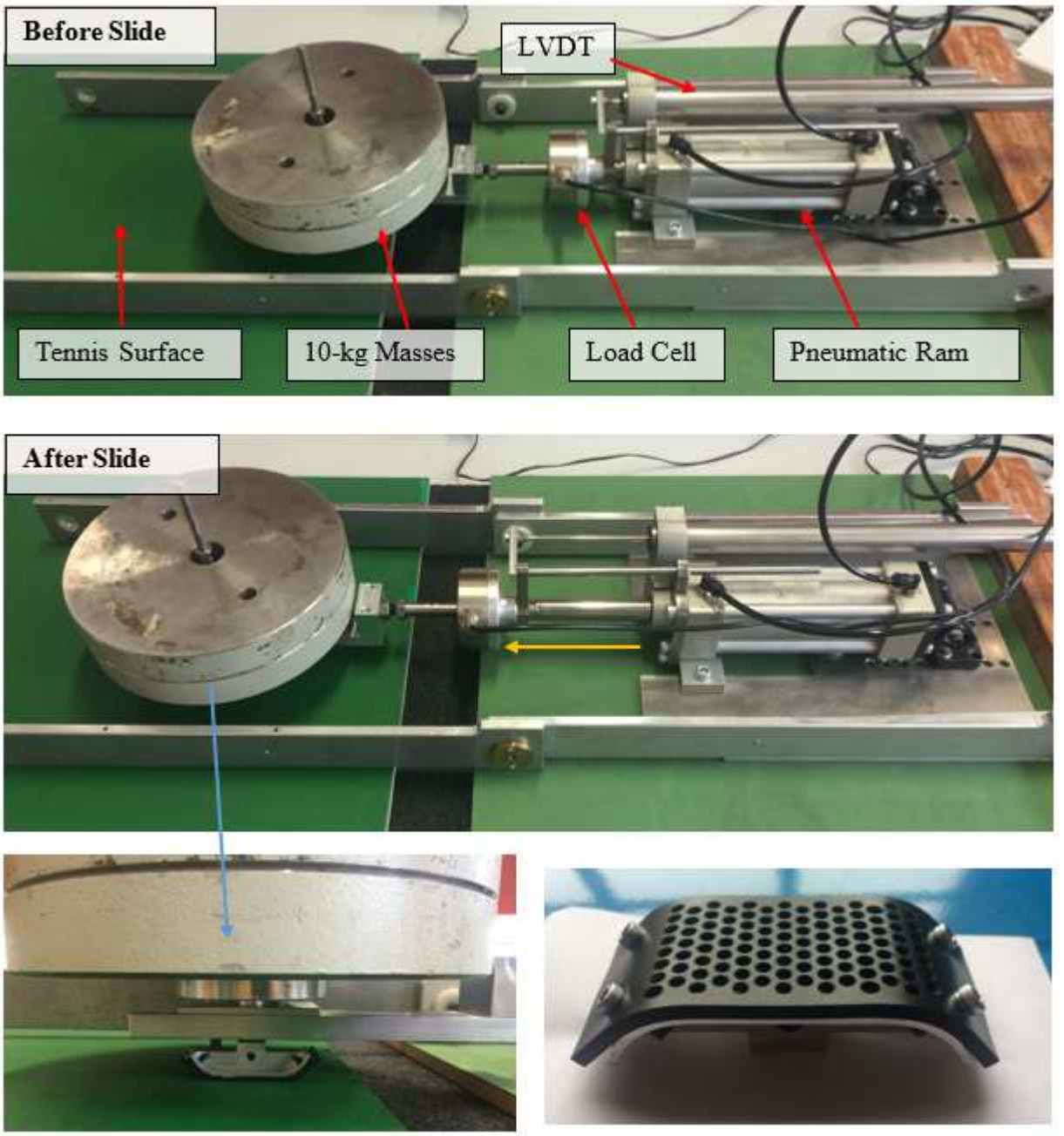

Figure 2. Photographs depicting PPR setup before (top) and after (center) a slide and the slider (bottom). The slide distance is 10 cm.

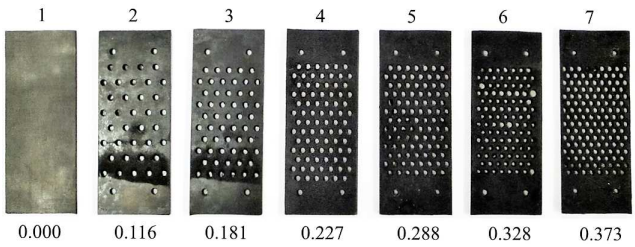

Figure 3. Photograph of holed-rubber samples. Sample numbers appear above the samples; area ratios appear below the samples. Each sample measures $3.0\,\text{cm} \times 7.9\,\text{cm}$ and has a thickness of 3 mm.

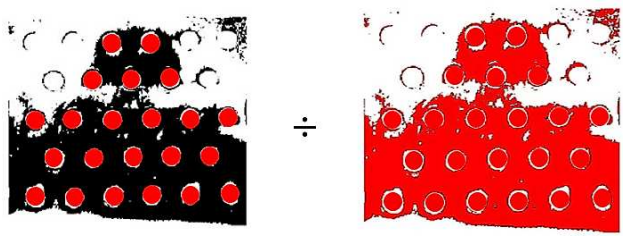

Figure 4. Visualization of area ratio, found by dividing the red area on the left by the red area on the right.

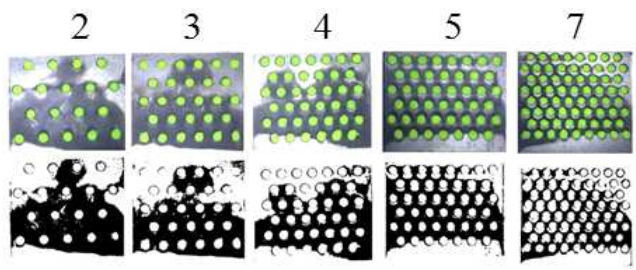

Figure 5. Photographs depicting wear (top) and images processed via thresholding (bottom). Sample numbers appear above samples.

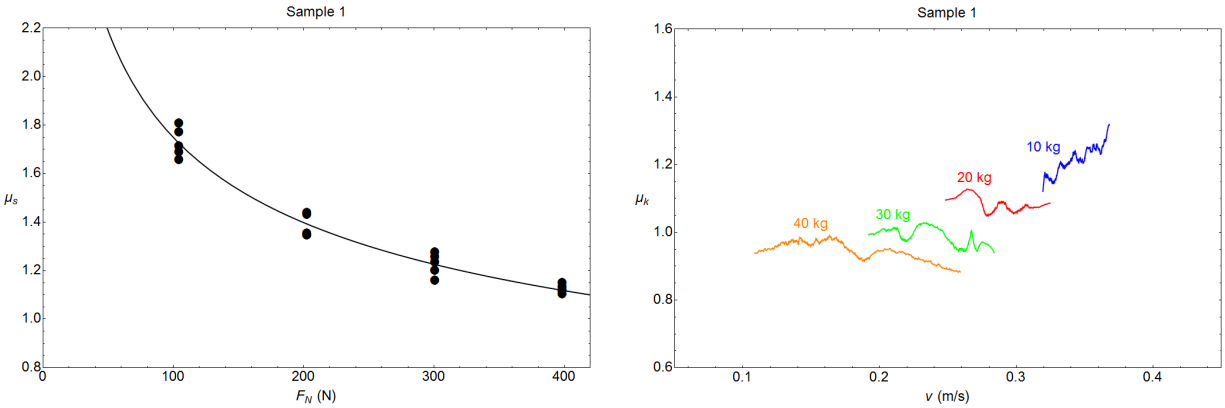

Figure 6. Sample 1 results. Left: Coefficient of static friction versus normal force. Fitting equation is shown. Right: Coefficient of kinetic friction versus speed.

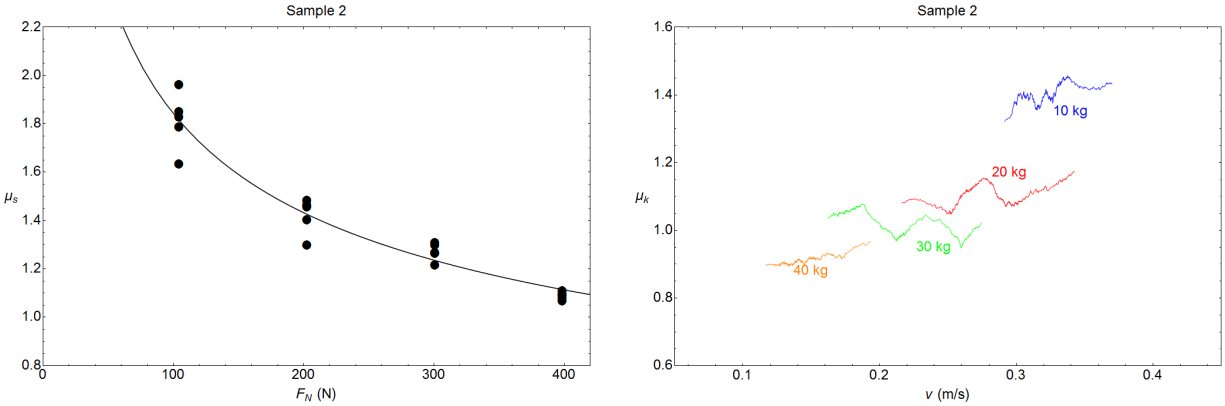

Figure 7. Sample 2 results. Left: Coefficient of static friction versus normal force. Fitting equation is shown. Right: Coefficient of kinetic friction versus speed.

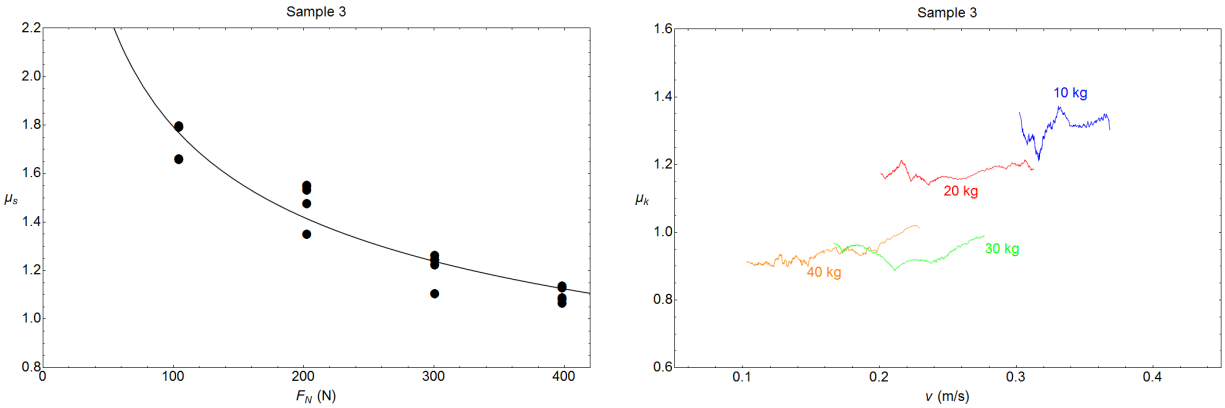

Figure 8. Sample 3 results. Left: Coefficient of static friction versus normal force. Fitting equation is shown. Right: Coefficient of kinetic friction versus speed.

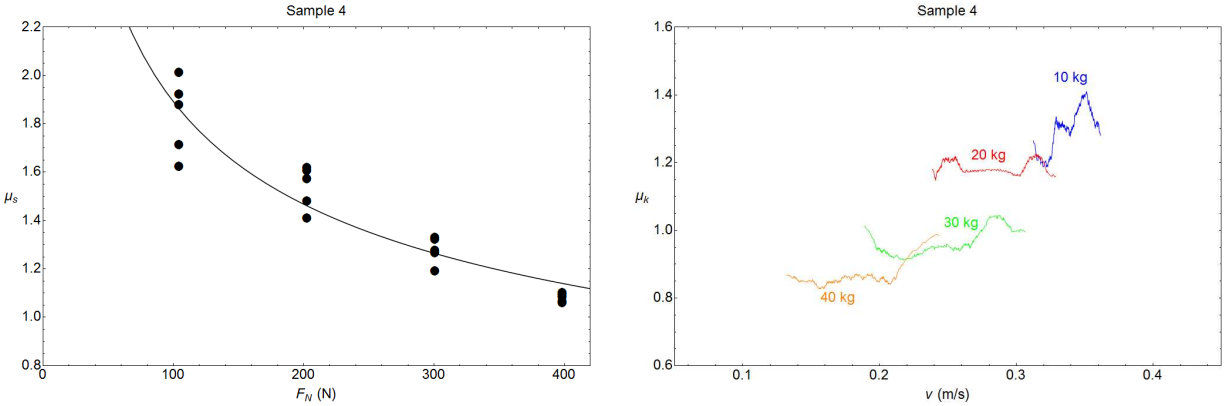

Figure 9. Sample 4 results. Left: Coefficient of static friction versus normal force. Fitting equation is shown. Right: Coefficient of kinetic friction versus speed.

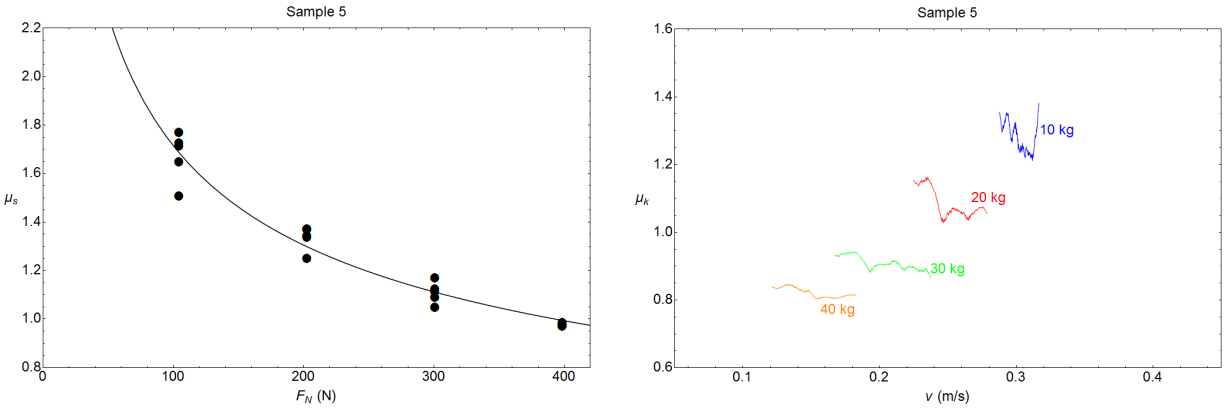

Figure 10. Sample 5 results. Left: Coefficient of static friction versus normal force. Fitting equation is shown. Right: Coefficient of kinetic friction versus speed.

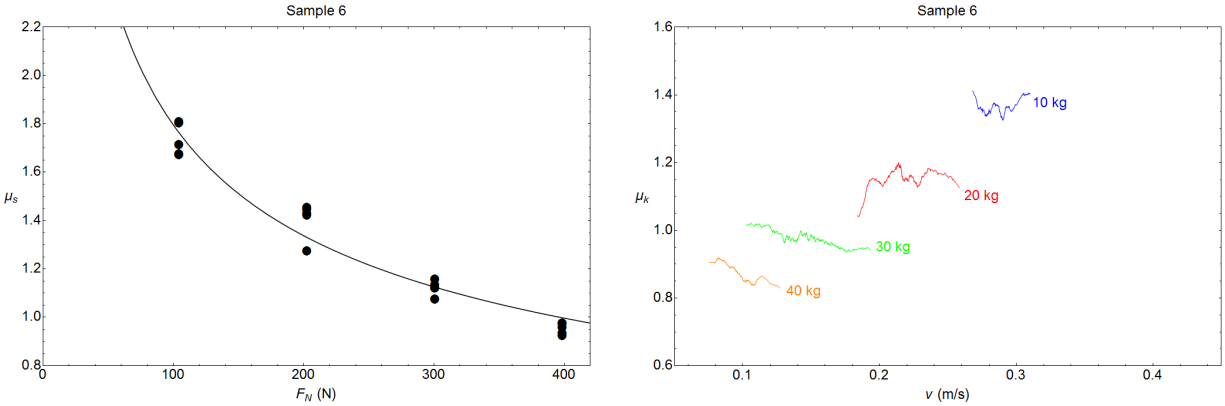

Figure 11. Sample 6 results. Left: Coefficient of static friction versus normal force. Fitting equation is shown. Right: Coefficient of kinetic friction versus speed.

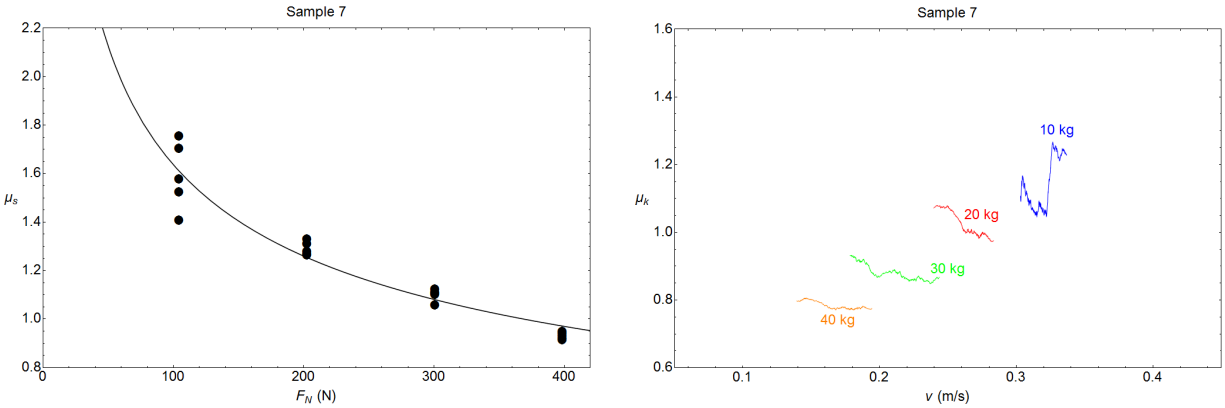

Figure 12. Sample 7 results. Left: Coefficient of static friction versus normal force. Fitting equation is shown. Right: Coefficient of kinetic friction versus speed.

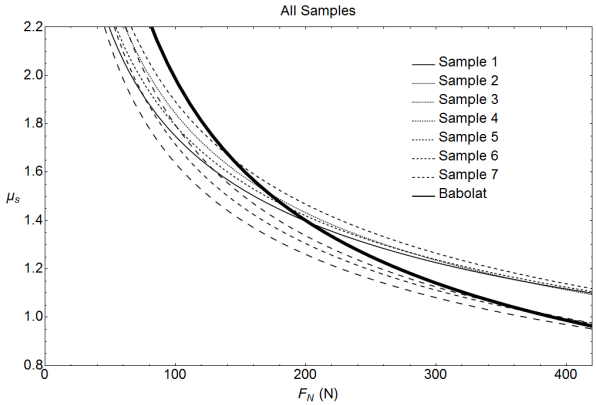

Figure 13. Fitting functions for coefficient of static friction. Spacing between dashes gets larger as sample number increases. Babolat shoe sample with dimples is shown with a thick curve.[1]

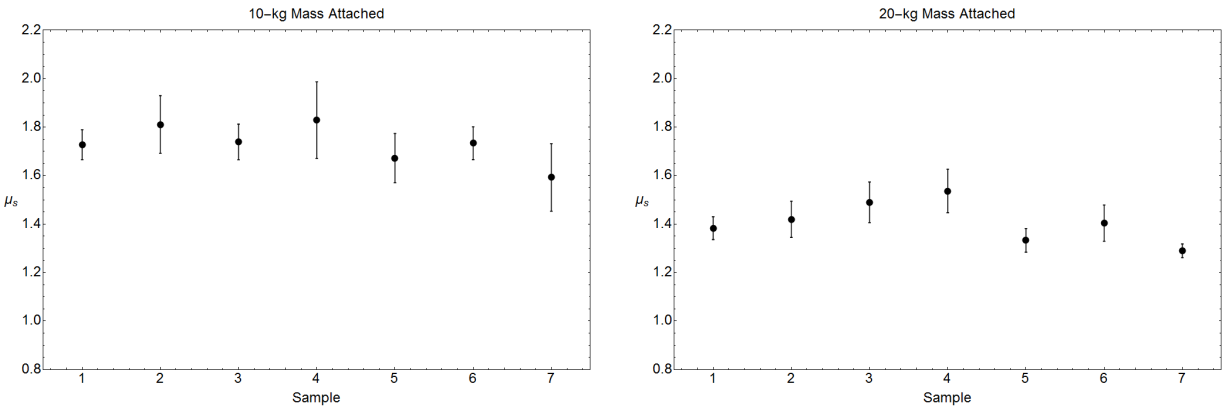

Figure 14. Average values of μ_s with standard errors for the seven samples when the 10-kg mass was attached (left) and when the 20-kg mass was attached (right).

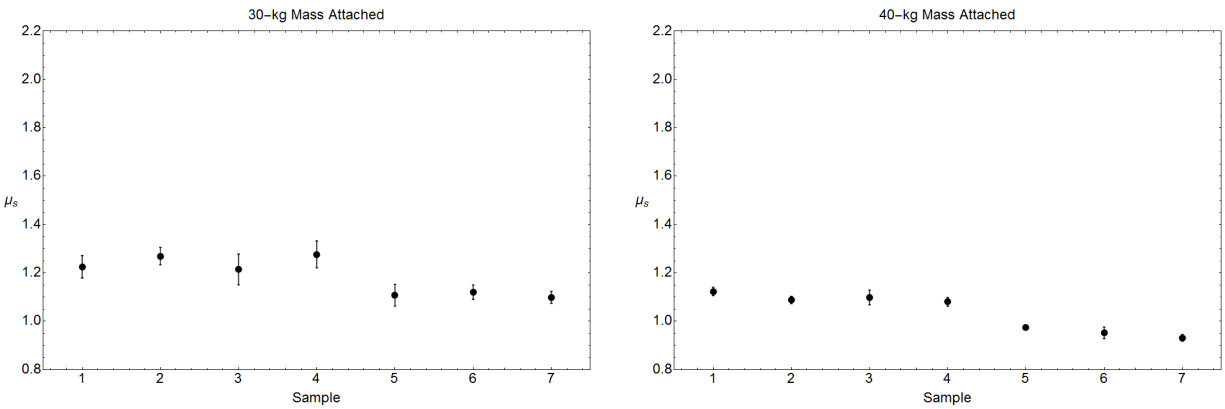

Figure 15. Average values of μ_s with standard errors for the seven samples when the 30-kg mass was attached (left) and when the 40-kg mass was attached (right).